Precision measurement of a low-loss cylindrical dumbbell-shaped sapphire mechanical oscillator using radiation pressure

J. Bourhill,* E. Ivanov, and M. E. Tobar

ARC Centre of Excellence for Engineered Quantum Systems, University of Western Australia, 35 Stirling Highway, Crawley, Western Australia 6009, Australia

(Received 27 February 2015; published 11 August 2015)

We present first results from a number of experiments conducted on a 0.53-kg cylindrical dumbbell-shaped sapphire crystal. Here we report on an optomechanical experiment utilizing a modification to the typical cylindrical architecture. Mechanical motion of the crystal structure alters the dimensions of the crystal, and the induced strain changes the permittivity. These two effects result in parametric frequency modulation of resonant microwave whispering gallery modes that are simultaneously excited within the crystal. A microwave readout system is implemented, allowing extremely low noise measurements of this frequency modulation near our modes of interest, having a phase noise floor of -165 dBc/Hz at 100 kHz. Fine tuning of the crystal's suspension has allowed for the optimization of mechanical quality factors in preparation for cryogenic experiments, with a value of $Q = 8 \times 10^7$ achieved at 127 kHz. This results in a $Q \times f$ product of 10^{13}, equivalent to the best measured values in a macroscopic sapphire mechanical system. Results are presented that demonstrate the excitation of mechanical modes via radiation pressure force, allowing an experimental method of determining the transducer's displacement sensitivity df/dx and calibrating the system. Finally, we demonstrate parametric backaction phenomenon within the system. These are all important steps towards the goal of achieving quantum limited measurements of a kilogram-scale macroscopic device for the purpose of detecting deviations from standard quantum theory resulting from quantum gravitational effects.

DOI: 10.1103/PhysRevA.92.023817 PACS number(s): 42.79.Jq, 42.50.Wk, 43.38.Zp

I. INTRODUCTION

The field of optomechanics is producing many exciting results, e.g., extremely precise sensors with applications in a wide variety of fields, including sensitive detection of previously immeasurable signals [1–7], quantum information processing [8,9], and tests of fundamental quantum theories, including potential tests of quantum gravity [10–15] and the detection of gravity waves [16–18]. The majority of work in this area is based on microscopic or mesoscopic resonators [19–22], which have the advantage of extremely low mass and therefore relatively large optomechanical coupling factors, allowing for a plethora of interesting physics to be investigated. In particular, the quantum regime of mechanical motion (the so-called "standard quantum limit") is far more accessible for these extremely small resonators. Great challenges arise when dealing with macroscopic resonators, and it has been shown that state-of-the-art technologies are required to approach observations of the quantum world in such resonators due to their significantly larger masses [23,24].

Despite this fact, there are numerous motivations for working in the "large-mass" regime. First and foremost, if one were to succeed in making the laws of quantum mechanics govern the behavior of human-scale objects, one would be able to look at a very strange quantum world with objects of far larger size, something that has never before been achieved and would be a momentous confirmation of quantum theory. In addition to this, proposed methods for beating the standard quantum limit of displacement uncertainty require the use of a squeezed state of light, placing all the uncertainty in the amplitude quadrature, hence enhancing the precision in the phase quadrature [25,26]. This becomes tenable only when the resulting increase in amplitude fluctuations and hence backaction noise minimally "kick" a resonator, i.e., if one uses low incident light power or the resonator has a large mass.

Finally, a recent proposal by Pikovski *et al.* [11] suggests that the standard Heisenberg uncertainty relationship and associated commutation relation between an oscillator's position and momentum may be altered by quantum gravitational effects, which could be detectable by macroscopic mechanical oscillators. Marin *et al.* [12] set an upper limit for possible Planck-scale modifications on the ground-state energy of an oscillator with the ton-scale gravitational wave detector AURIGA. The deformation of the standard uncertainty relationship is quantified by an expression β_0, which will have an upper limit set by the experimental parameters. For the parameters of the resonator discussed here, if it were simply cooled using standard dilution refrigeration technology to 20 mK (without the use of parametric cooling or active feedback cooling [20,27,28]), the upper limit placed on this modification is equal to that of the best reported results.

The essential requirement for the observation of optomechanical effects is to generate coupling between phonons and photons within a resonant structure. This coupling can take many forms, including variations in path length of a Fabry-Perot resonator via a movable mirror (such as the LIGO experiment) [16,29], oscillations of a cantilever capacitively coupled to two electrodes [30], "membrane-in-the-middle"-type experiments [31,32], or, as in the present work, crystalline resonators, which can support both optical and microwave resonant fields and mechanical modes [33,34]. All of these systems function via mechanical effects causing a disturbance to an optical field, which can be measured as a frequency shift. In the case of a macroscopic whispering gallery mode (WGM) resonator, its frequency is sensitive to changes in path length

*jeremy.bourhill@uwa.edu.au

(i.e., the circumference and height of the cylinder) and strain in the crystal lattice, both of which are induced by mechanical motion. The latter effect is, in fact, the more dominant mechanism [23,24]. These lattice vibrations can be caused by thermal phonons within the resonator at room temperature.

The quantities one needs to minimize for achieving quantum limited resolution of an optoacoustic device, given a fixed mass and resonant frequency, are its temperature and phase noise, while the quantities that need to be maximized are the mechanical and optical Q factors and frequency sensitivity to displacement (G). Electromagnetic sapphire oscillators offer excellent phase noise performance, as evidenced by their long-standing history in clock technology [35,36]. The extremely high electromagnetic Q factors ($\sim 10^8$) are also accompanied by an equally important large mechanical Q factor ($\sim 10^8$–10^9). Therefore, sapphire optoacoustic devices present as an excellent candidate for achieving a quantum limited macroscopic mechanical oscillator.

II. SAPPHIRE RESONATOR: GEOMETRY AND MODES OF VIBRATION

The sapphire resonator studied takes the form of a dumbbell-shaped cylinder and is herein referred to as the "split bar" (SB) resonator, with its dimensions outlined in Fig. 1(a). It is suspended via a wire loop around the central "neck," which is 14.9 mm long and has a radius of 7.5 mm. This shape was chosen to isolate the point of suspension from the mechanical motion in order to maximize mechanical Q factors. The crystal is high-quality HEMEX-grade sapphire and was grown using the heat exchange method by Crystal Systems, USA, cut to dimensions, and then optically polished.

The SB is both an electromagnetic and mechanical resonator. Its cylindrical shape permits high-Q-factor WGMs to be excited at microwave frequencies and, via the mechanism explained above, the coupling between acoustic and electromagnetic modes required for the observation of optomechanical effects is achieved.

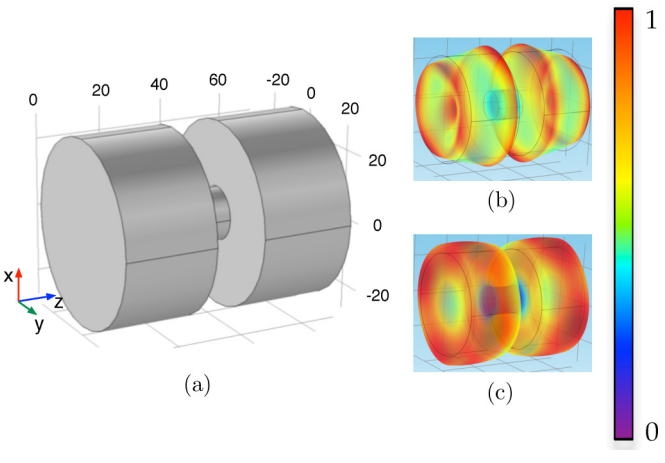

FIG. 1. (Color online) (a) Graphical representation of the SB resonator modeled using FEM. Lengths shown are in millimeters. Normalized displacement field of the 95-kHz (b) and 127-kHz (c) resonant mechanical modes.

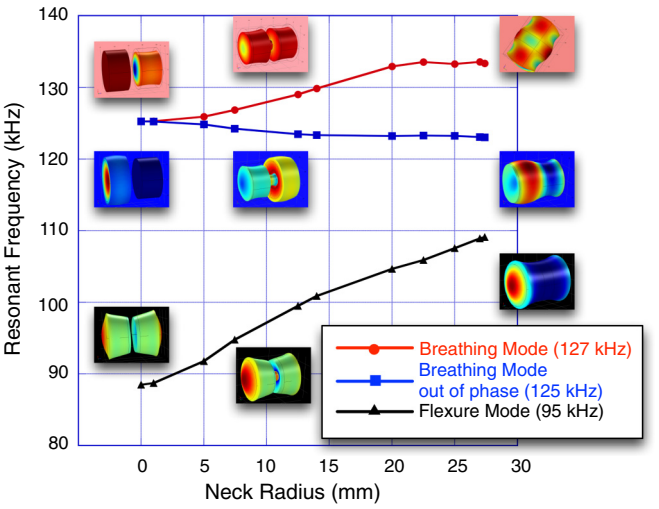

FIG. 2. (Color online) Three relevant mechanical-mode families' resonant frequencies as functions of neck diameter. The SB resonator has a neck diameter of 14.92 mm. By examining the two limiting cases of the SB (i.e., neck diameter 0 mm, corresponding to two separate cylinders, and neck diameter 27.4 mm, corresponding to one large cylinder; the origin of each mode can be correctly identified).

The SB resonator was modeled using finite element modeling (FEM) software (COMSOL) to identify suitable mechanical modes within the crystal. Given the nonuniformity of the dimensions, the eigenfrequencies of the resonant modes were solved for varying neck diameters, ranging from the limiting cases of two separate cylinders of height 27.9 mm to a single uniform cylinder of height 70.4 mm, in order to identify the correct families of the modes.

In a majority of optomechanical experiments that deal with a cylindrical architecture, it is the fundamental longitudinal mode that couples most strongly to the optical field [12,27,37–39]. This will be a relatively low-frequency mode in comparison to others; for a full cylinder of the SB resonator's dimensions, the fundamental mode is shown by the right-hand limit of the black curve in Fig. 2. By removing the central ring of sapphire to form the dumbbell structure, we observe that the mode that most closely mimics the motion of the fundamental longitudinal mode is the 127-kHz mode, referred to as the "breathing mode." This originates from a higher-order mode than the fundamental longitudinal mode. Therefore, by removing a small portion of mass (the removed ring weighs $\sim$120 g), we have increased the operating mechanical frequency by $\sim$18 kHz, which is more than could be achieved by reducing either the radius or the length (or both) of a full cylinder to replicate the same loss of mass. Thus, by moving to a dumbbell architecture, we have achieved a higher mechanical frequency for a given mass of sapphire than otherwise possible. This is a nontrivial result, as the resulting increase in phonon energy ($\hbar\Omega_m$) results in a lower thermal phonon occupation number for a given temperature.

From Fig. 2 one can see that the in-phase and out-of-phase breathing modes (127- and 125-kHz modes, respectively) are degenerate for the case of two separate crystals, but when they become joined, their frequencies tune in opposite directions. These modes become very different in the limiting case of a full

cylinder. Each one of the modes in Fig. 2 has been detected with frequencies in very good agreement with the modeled values (<1%). This article will mainly deal with the 95-kHz mode (black curve) and the 127-kHz mode (red curve), as they have the two highest Q factors. The low Q factor observed for the 125-kHz mode is predicted by the modeling due to a large amount of displacement at the suspension point on the neck of the dumbbell, resulting in larger suspension losses. The modeling also allows for the calculation of the effective masses of each mode, the 127-kHz mode being 0.306 kg, while the 95-kHz mode is 0.260 kg.

From the FEM, it is possible to obtain deformation gradients ($\frac{dz}{z}$, $\frac{dr}{r}$, $\frac{d\phi}{\phi}$) and total displacement curves for each of the modes, allowing an estimate of the WGM frequency sensitivity to each different mechanical mode family. For simplicity, this is done using a model of only one cylindrical end of the SB, at the mode of interest's corresponding eigenfrequency in this limiting case, as depicted in Fig. 2.

To determine the magnitude of frequency variations due to mechanical vibrations ($\frac{df}{dx}$) of any particular WGM, we expand on the method used by Locke *et al.* [23]. The frequency of WGMs in cylindrical sapphire, assuming that the crystal axis (c axis) is aligned with the z axis, is dependent upon four variables: the permittivities of the crystal perpendicular and parallel to its c axis, $\varepsilon_\perp$ and $\varepsilon_\parallel$, respectively (sapphire is an anisotropic crystal), and the crystal's dimensions (diameter, D, and length, L).

The frequency sensitivity of the WGM can be calculated from

$$\frac{z}{f}\frac{df}{dz} = \nu\left[\left(M_r p_{\varepsilon_r} + M_\phi p_{\varepsilon_\phi}\right)K_{\varepsilon_\perp} + p_D\right] - M_z p_{\varepsilon_z} K_{\varepsilon_\parallel} - p_L, \quad (1)$$

where p_i are the normalized tuning coefficients of the WGM frequency with respect to the variable i (i.e., $p_i = |\frac{\delta f^{\text{res}}}{\delta i}|\frac{i}{f}$), ν is Poisson's ratio, K_{ε_i} represents the strain dependence of permittivity (i.e., $K_{\varepsilon_\parallel} = \frac{d\varepsilon_\parallel}{dz}\frac{L}{\varepsilon_\parallel}$ and $K_{\varepsilon_\perp} = \frac{d\varepsilon_\perp}{dr}\frac{D}{2\varepsilon_\perp}$), and M_i is the displacement modification factor and represents the overlap of electric field $[\underline{E_i}(r,z,\phi)]$ and strain $[S_i(r,z,\phi)]$ in the i direction,

$$M_i = \frac{\int_V S_i(r,z,\phi)\varepsilon_i \underline{E_i}(r,z,\phi)\underline{E_i^*}(r,z,\phi)drdzd\phi}{N_i}, \quad (2)$$

where N_i is a normalization constant.

Frequency sensitivity to changes in permittivity only occurs in the electrical component of the resonant microwave mode. This is due to the dependence of the E field on ε compared to a B field's dependence on μ, a direct result of Maxwell's equations. WGMs have two main polarizations: WGH (transverse magnetic whispering gallery) modes with dominant E_z, H_r, and H_ϕ field components and WGE (transverse electric whispering gallery) modes with dominant H_z, E_r, and E_ϕ components. Therefore, transduction in the SB will be primarily due to the strain induced in the direction of the WGM's E fields. Since $\nu = 0.3$ for sapphire, WGH modes are more strongly affected by mechanical motion.

Figure 3 depicts the method by which the M_z factors are calculated for the 95- and 127-kHz mechanical modes. The overlap of the electromagnetic and strain fields determines

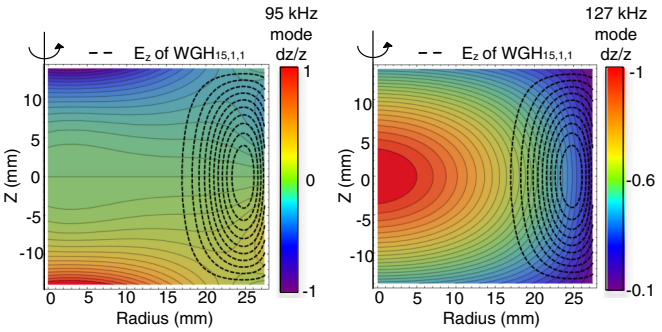

FIG. 3. (Color online) Overlap of $WGH_{15,1,1}$ E_z field and deformation gradient $\frac{dz}{z}$ used to calculate M_z modification factors in Eq. (1).

the magnitude of WGM frequency variations. It should be noted that the 95-kHz mode's deformation gradient is an antisymmetric function about $Z = 0$, and hence the mean strain is zero, compared to the symmetric 127-kHz mode. This results in effectively zero strain contribution to $\frac{df}{dx}$ in Eq. (1) for the 95-kHz mode; hence, the main component of transductance for this mode is expected to be a result from the physical change of boundary conditions.

Following the treatment used by Tobar and Mann [40,41], a mode-matching technique is used to determine the p_i values and the E-field distributions in each of the cylindrical coordinate directions. This can be done for both WGH and WGE modes with any number of azimuthal maxima. Then, taking the deformation gradients for the two mechanical modes produced in FEM, M_i values are determined to finally produce an estimate for $\frac{df}{dx}$, as shown in Table I.

With the parameters derived in this section, we can briefly make an assessment of the SB resonator's effectiveness in terms of its ability to compare various quantum gravity models [11,13–15]. As discussed by Marin *et al.* [12], a macroscopic oscillator could potentially detect modifications to the Heisenberg uncertainty relation caused by quantum gravitational effects [11] of the form

$$\Delta x \Delta p \geqslant \frac{\hbar}{2}\left[1 + \beta_0\left(\frac{\Delta p}{M_p c}\right)^2\right], \quad (3)$$

where M_p is the Planck mass ($M_p = 2.2 \times 10^{-8}$ kg) and c the speed of light. The figure of merit for any such experiment is the upper limit placed on β_0, which quantifies the deformation,

$$\beta_0 < 2\frac{k_B T}{\hbar\Omega_m}\frac{M_p}{m}\frac{M_p c^2}{\hbar\Omega_m}, \quad (4)$$

where m is the mass of the resonator, T its temperature, k_B is Boltzmann's constant, and Ω_m is the mechanical resonant

TABLE I. Calculated values for the $WGH_{15,1,1}$ mode and the 95- and 127-kHz mechanical modes.

$\Omega_0/2\pi$ (kHz)	M_z	M_r	M_ϕ	$\lvert df/dz\rvert$ (MHz/μm)
94.97	0[a]	0[a]	0[a]	0.085
127.07	0.38	0.0017	0.024	0.18

[a]A value of zero is due to the asymmetry of the 95-kHz mode strain curves.

frequency; hence, the first fraction defines the thermal phonon occupation number, n_t. For the SB resonator, if it were only cooled using conventional refrigeration technology to 20 mK, we obtain $\beta_0 < 6 \times 10^{33}$, equal in magnitude to the best reported results (see the comparison in [12]).

III. EXCITING MECHANICAL MODES AND MEASURING *Q* FACTORS

Initially, a piezoelectric actuator was used to excite the SB and therefore locate the resonant mechanical modes. The piezo was mounted to the SB's copper housing on a lid at one of the end faces and was not in direct contact with the crystal. This setup is shown in Fig. 4. The piezo driving frequency was chirped over a small frequency range (on the order of 1 kHz) to conduct a relatively broadband search for resonances around the predicted frequencies. However, under vacuum the only path for the acoustic excitation of this form is through the suspension wire and if the length of this wire is optimally tuned such that the driving frequency is nonresonant with the wire, the transmission of energy to the bar will be minimal and the modes difficult to excite. In addition to this, driving the piezo with a periodic chirp results in the reduced contrast of the resonant peak viewed on a network analyzer due to nonresonant excitation caused by shaking of the copper housing.

An alternative method for mechanical excitation is applying radiation pressure force (RPF) to the crystal by modulating the power of the amplitude modulated (AM) microwave signal at the mechanical resonance frequency (see Fig. 10). Once the AM is switched off the SB will continue to resonate mechanically, with its amplitude ringing down with a characteristic time constant, τ, which can be used to calculate the Q factor of the mode ($Q_m = \pi \tau f_{\text{mech}}$). The results of this ringdown technique are shown in Fig. 5.

When used together, these two techniques provide an effective and simple method for the excitation of mechanical modes and Q factor measurements; the piezo is chirped to find the exact location of the resonance (within one bandwidth, on the order of mHz), and the input microwave signal is then

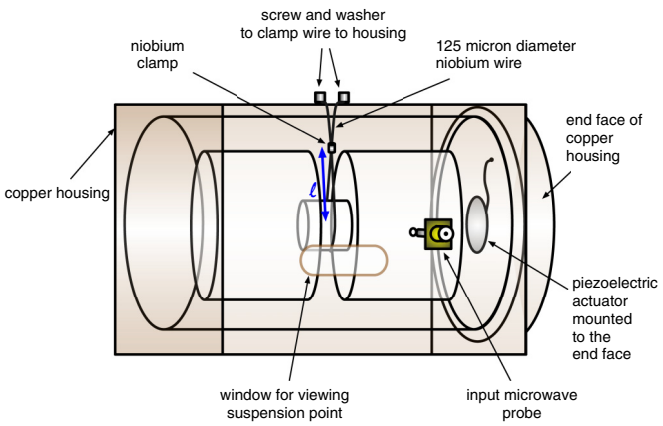

FIG. 4. (Color online) A diagram of the SB suspended inside a copper cavity. The length of wire from the point of contact with the crystal neck to the position of the niobium clamp, labeled by a blue double arrow, is the length that must be tuned.

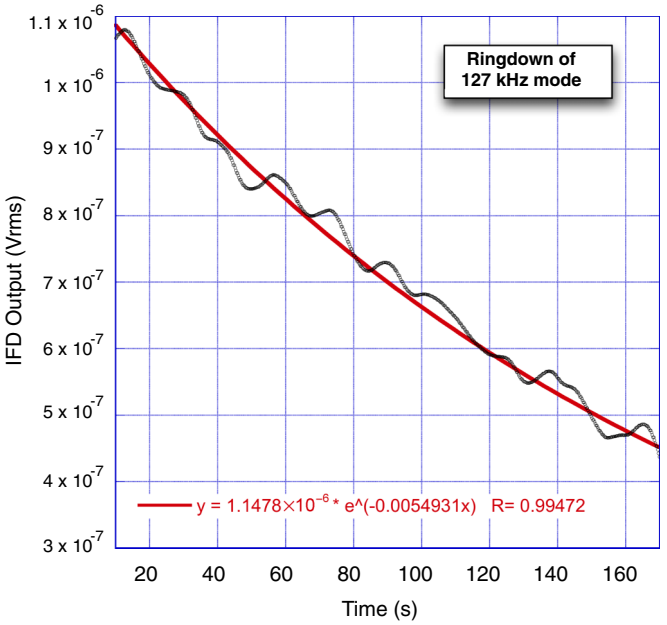

FIG. 5. (Color online) Mechanical Q factor can be obtained from fitting the ringdown of the mechanical mode, measured by the output of the frequency discriminator. The low-frequency modulation of the output signal is caused by a low-frequency "rocking motion" of the bar as it oscillates as a pendulum about its suspension point, both along its central axis and rotating about it.

AM modulated at this resonant frequency for a period of time longer than the ringdown time of the mode (to allow full excitation). The AM modulation is then switched off, and finally the amplitude of the resulting peak is tracked over a time period of about 200 s. Figure 5 shows a measured value of $\tau = 1/0.0052$ s for the 127-kHz mode, corresponding to a mechanical Q factor of 7.7×10^7.

By varying the amount of modulation on the incident power and measuring the peak amplitude immediately after AM modulation has been switched off (provided RPF has been applied for a sufficiently long period of time that the resonator is in a quasistatic regime), one can experimentally determine a value for df/dx for each of the mechanical modes, and compare with predicted values, as will be shown.

Treating the mechanical sapphire resonator as a standard harmonic oscillator, we have

$$m_{\text{eff}} \frac{d^2x(t)}{dt^2} + m_{\text{eff}} \Gamma_m \frac{dx(t)}{dt} + m_{\text{eff}} \Omega_m^2 x(t) = F_{\text{ext}}(t), \quad (5)$$

which has the standard solution for displacement:

$$\delta x(\omega) = \frac{1}{m_{\text{eff}}} \frac{F_{\text{ext}}(\omega)}{\Omega_m^2 - \omega^2 - i\omega\Gamma_m}. \quad (6)$$

Here m_{eff} is the effective mass of the bar in its resonant mechanical mode of frequency Ω_m, $\Gamma_m = \Omega_m/Q_m$ is the mechanical decay rate, and F_{ext} is some applied force. We can relate this displacement to a physically observable quantity, i.e., the voltage produced at the mixer output of the microwave readout system:

$$\delta u(\omega) = \delta x(\omega) \left(\frac{du}{df}\right)\left(\frac{df}{dx}\right). \quad (7)$$

We wish to solve this equation for the case of $F_{\rm ext}$ originating from applied RPF. The expression for this can be found by differentiating the standard interaction Hamiltonian for an optomechanical system with respect to position [42],

$$\hat{H}_{\rm int} = -\hbar g_0 \hat{a}^\dagger \hat{a}(\hat{b} + \hat{b}^\dagger), \tag{8}$$

where $\hat{a}^\dagger$ and $\hat{a}$ are the photon raising and lowering operators, respectively, $\hat{b}^\dagger$ and $\hat{b}$ are the phonon raising and lowering operators, respectively, and g_0 is the single photon optomechanical coupling:

$$g_0 = G x_{\rm ZPF} = \frac{d\omega}{dx} x_{\rm ZPF}, \quad x_{\rm ZPF} = \sqrt{\frac{\hbar}{2 m_{\rm eff} \Omega_m}}. \tag{9}$$

We can define the position operator $\hat{x}$ as

$$\hat{x} = x_{\rm ZPF}(\hat{b} + \hat{b}^\dagger), \tag{10}$$

which will allow us to solve for $F_{\rm ext}$:

$$F_{\rm ext}(t) = -\frac{d\hat{H}_{\rm int}}{d\hat{x}} = \hbar G \hat{a}^\dagger \hat{a} = \hbar \frac{d\omega}{dx} n_{\rm cav}. \tag{11}$$

Here $n_{\rm cav}$ is the number of photons inside the cavity and can be solved by dividing the total energy inside the cavity [43] by the energy of a single photon, as

$$n_{\rm cav} = \frac{E_{\rm WGM}}{E_{\text{single photon}}}, \quad E_{\text{single photon}} = \hbar\omega,$$
$$E_{\rm WGM} = P_{\rm inc} \frac{Q_e}{\omega} \frac{4\beta_1}{(1+\beta_1+\beta_2)^2} \frac{1}{1 + 4Q_e^2\left(\frac{\omega-\omega_e}{\omega_e}\right)^2}, \tag{12}$$

where $P_{\rm inc}$ is the power of the incident microwave signal at frequency ω_e, Q_e is the quality factor of the WGM, and β_1 and β_2 are the couplings between the WGM resonance and the input and output microwave probes, respectively.

Assuming we are driving the microwave input at the WGM resonance ($\omega = \omega_e$), we finally arrive at an expression for the RPF inside the sapphire:

$$F_{\rm ext}(t)|_{\omega=\omega_e} = \frac{d\omega}{dx} \frac{P_{\rm inc}(t) Q_e}{\omega_e^2} \frac{4\beta_1}{(1+\beta_1+\beta_2)^2}. \tag{13}$$

As a side note, this equation is identical to that obtained by Locke *et al.* [38] when modeling the optomechanical system as an LCR circuit with a modulated capacitance.

Assuming the incident power is modulated at Ω_m, we can derive an equation for the voltage output by the microwave readout system,

$$\delta u(\Omega_m) = \pi\sqrt{2\pi}\left(\frac{du}{df}\right)\left(\frac{df}{dx}\right)^2 \chi_{\rm WGM}\chi_{\rm mech}\delta P, \tag{14}$$

where $\chi_{\rm WGM} = \frac{4\beta_1}{(1+\beta_1+\beta_2)^2}\frac{Q_e}{\omega_e^2}$ and $\chi_{\rm mech} = \frac{Q_m}{m_{\rm eff}\Omega_m^2}$.

From Eq. (14), we can observe that by measuring du/dP, one can determine a value for df/dx experimentally. The results of this measurement are shown in Fig. 6, and every other value in Eq. (14) can be directly measured from the system. From the gradient of these two curves, $df/dx_{127} = 0.19$ MHz/μm and $df/dx_{95} = 0.05$ MHz/μm.

The value for the 127-kHz mode is in very good agreement with the predicted value (~6% error), while the 95-kHz mode is measured to be 40% smaller than its estimated value (see Table I). This can be attributed to the assumption that there was no strain induced contribution to the 95-kHz transduction in the simulation. As the WGM used has ~95% of its E field in the z direction, any strain contribution would arise mainly in this axis, which would subtract from the value obtained from purely dimensional changes [see Eq. (1)]. For example, a strain contribution 1/10th the magnitude of the 127-kHz mode would result in the predicted value being in good agreement with the measured value. This arises in practice because the strain curve of the 95-kHz mode is not a pure odd function, and the WGM is not a pure even function about $Z = 0$ (see Fig. 3), as was assumed when treating the interaction of the two modes with Eq. (1), which, in addition, is only an approximation to first order. Some small perturbations of these two symmetries will result in a small strain contribution to df/dx_{95}, which will subtract from the purely dimensional contribution.

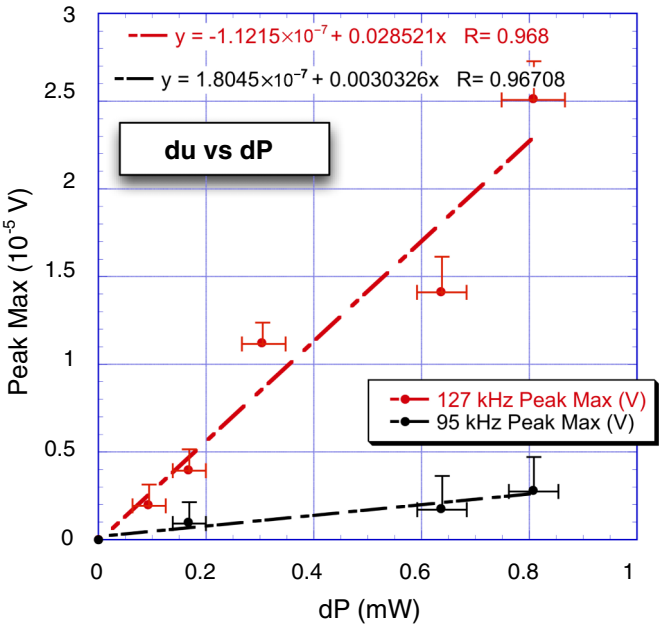

FIG. 6. (Color online) Measurements of maximum peak amplitude of readout system output (proportional to displacement) to varying amounts of RPF.

IV. OPTIMIZING MECHANICAL Q FACTORS

Energy dissipated through the suspension is generally the dominant loss mechanism in optomechanical systems, as long as they are held under vacuum.

The wire-loop suspension used to hold the SB is a method traditionally used by the gravitational wave community, which has been shown to achieve the highest mechanical Q factors over other suspension schemes [44] (see the comparison of suspension techniques depicted in Fig. 9). Braginsky *et al.* [44] modeled the losses in such a suspension as

$$\frac{1}{Q_s} = \frac{2\rho_w A_w l_w}{m_{\rm eff} Q_w} \frac{x_{\rm ext}^2}{x_0^2} \times \left[1 + \frac{1}{2}\left(\frac{\omega_m l_w}{v_w Q_w}\right)^2 - \cos\left(\frac{2 l_w \omega_m}{v_w}\right)\right]^{-1}, \tag{15}$$

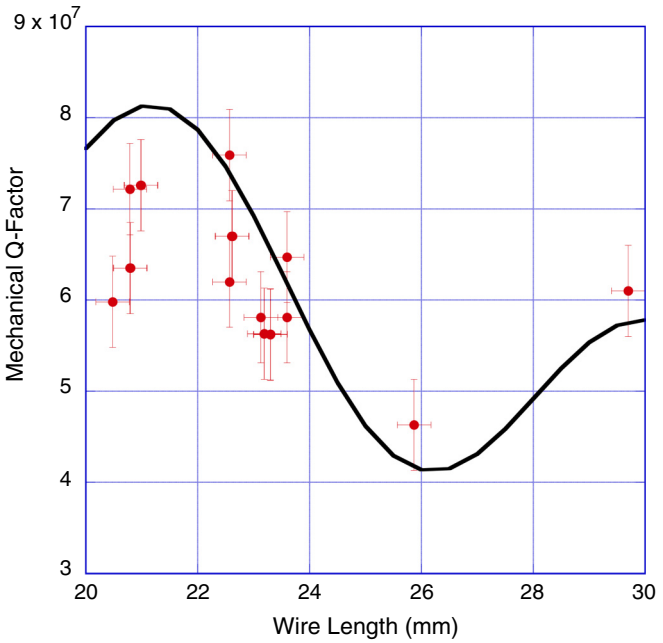

FIG. 7. (Color online) Measured mechanical Q factors as the length of the Nb suspension wire is altered. Lengths are measured from the angle made by the suspension. A speed of sound in Nb of 2200 m/s produces the best fits, in agreement with quoted values for the speed of transverse waves in a thin Nb rod at 20 °C.

where ρ_w, A_w, l_w, Q_w, and v_w are the density, cross-sectional area, length, mechanical Q factor, and velocity of sound of the wire, respectively, and x_0 and x_{ext} are the amplitude of vibration of the resonator and the amplitude at the point of contact with the wire, respectively. Equation (15) predicts a periodic variation in Q factors as the length of the wire (shown in blue in Fig. 4) is changed. However, Eq. (15) has only been shown to provide qualitative agreement with experimental results, as the loss mechanism is far more complicated than this simple model.

Two different wires were trialled for the suspension system: an 80-μm-diameter tungsten wire and a 125-μm-diameter niobium wire, with better results being achieved with the latter due to its higher intrinsic Q_w. The niobium clamp (shown in Fig. 4) is necessary to keep enough friction around the neck of the SB to maintain balance, but can also be used to alter the length of the wire by moving its position. The clamps are made by cutting small lengths of 0.65-mm-diameter niobium tubing. Tests were made with both clamped and unclamped pieces of tubing, with the former producing higher Q factors due to the boundary condition in the wire resonance being fixed.

Results of varying wire length are presented in Fig. 7. Each experimental data point represents an entirely new wire suspension, as the clamping technique used fixes the wire's length. As such, it is possible for surface conditions and the loop's position along the z axis to change between measurements. Therefore, each of the data points in Fig. 7 represents a lower limit of Q factor for any given wire length.

Braginsky *et al.* [44] states that there is only a qualitative agreement between Eq. (15) and the experimental data, with measured Q factors being larger than the predicted values by almost a full order of magnitude. This is mainly due to resonator vibrations at the point of contact with the suspension wire being only partially transmitted to the wire. As such, we insert an additional term inside the square brackets of Eq. (15) to represent coupling between the wire and the crystal. It takes the form of $1/\xi$. It should also be noted that the second term inside the square brackets of Eq. (15) is much less than 1 and can therefore be neglected. The experimental results are then fitted with the equation

$$Q_s = \frac{m_{\text{eff}} Q_w}{2\rho_w A_w l_w} \frac{x_0^2}{x_{\text{ext}}^2}\left[1 + \frac{1}{\xi} - \cos\left(\frac{2l_w\omega_m}{v_w}\right)\right], \tag{16}$$

which is shown in black in Fig. 7 and provides a good bound of the measured Q factors given the fitted values of $Q_w = 8.5 \times 10^5$ and $\xi = 0.31$.

Figure 8 shows the dependence of mechanical Q factors on pressure, as predicted by the equation [45]

$$\frac{1}{Q_{\text{gas}}} \approx \frac{PA}{M\omega_0}\sqrt{\frac{\mu}{k_b T}}, \tag{17}$$

where P is pressure (in Pascals), A is the surface area of the mechanical resonator, M is its mass, and μ is the mass of molecule comprising majority of the gas in question. As can be seen from Fig. 8, below a certain threshold pressure, residual gas damping is no longer the dominant loss mechanism, with Q factors of close to 10^8 demonstrated.

Throughout the literature regarding wire-loop suspensions, it is often noted that by applying a small layer of lubrication (most commonly animal fat is used) to the surface of the mechanical resonator at the point of suspension, significant improvements in Q factors can be achieved [24,37,44]. Previously, at room temperature, Q factors on the order of 10^8 and $Q_m \times f \geqslant 6 \times 10^{12}$ have only been achieved with some form of lubrication, and this is therefore a strategy that could be

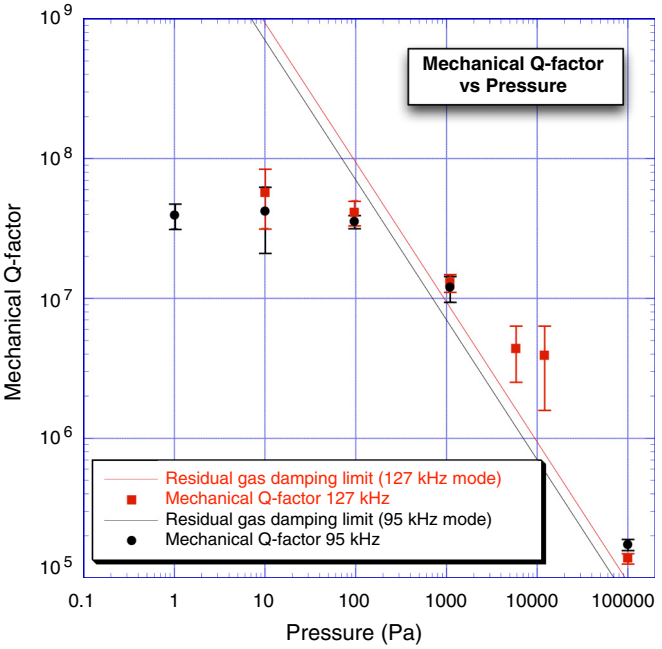

FIG. 8. (Color online) Mechanical Q factor of the 127- and 95-kHz modes vs pressure. Residual gas damping limits as predicted by Eq. (17).

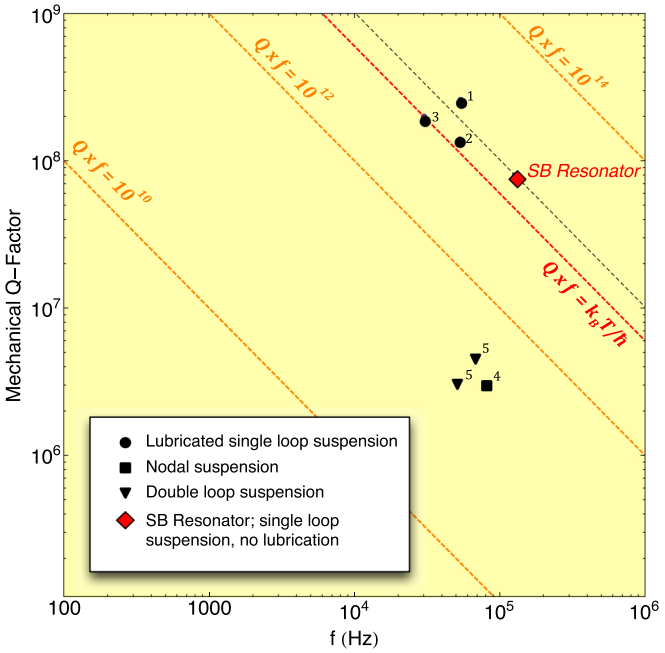

FIG. 9. (Color online) Reported mechanical quality factors and resonant frequencies of published experiments with sapphire-bar optomechanical systems at room temperature: 1, Ref. [37]; 2, Ref. [24]; 3, Ref. [44]; 4, Ref. [46]; 5, Ref. [39]. The experiments are differentiated by their suspension techniques. The black dashed line represents the $Q \times f$ product of the SB.

implemented in the immediate future of this work. However, even without lubrication, the present work corresponds to a $Q_m \times f$ product of 10^{13}, equivalent to the best measured values of sapphire acoustic systems, as depicted in Fig. 9. This product is considered a figure of merit for acoustic resonant systems, as it is a direct measure of the degree of decoupling from the thermal environment. Specifically, $Q_m \times f > k_b T/h$ is the condition for neglecting thermal decoherence over one mechanical period and is considered the minimum requirement for quantum optomechanics [42]. At room temperature, this lower limit is equal to 6×10^{12}, and is represented in Fig. 9 by the red dashed line.

Importantly, our results are consistent with the best reported values measured at room temperature in sapphire, most likely limited by the quality of the crystal [24,44]. Thus, this result demonstrates that equivalent performance to state-of-the-art sapphire acoustic systems can be achieved with a modified cylindrical structure. All other results presented in Fig. 9 are achieved using modes in full cylinders in the limiting case shown on the right-hand side of Fig. 2. This is the first time optomechanics in a sapphire bar has been attempted with a modified architecture.

By cooling the SB, the coupling between the suspension and crystal will decrease, resulting in the suspension losses decreasing. Q factors on the order of 10^9 have been achieved using wire suspended sapphire at liquid helium temperatures [44]. So while a maximum value of $\sim 8 \times 10^7$ has been achieved thus far, we are optimistic about improving this.

By following the analysis of Braginsky *et al.* [44], it can be shown that a minimum temperature of 17 mK would be required for the SB to achieve quantum limited measurements, even if the Q factor were to show no improvement at lower temperatures. This is not to be confused with achieving ground-state cooling, as at this temperature $k_B T > \hbar\omega$, but would nonetheless allow the resolution of a single quantum of acoustic energy: a phonon. Cooling the SB to the mechanical ground state is an extremely ambitious goal and will require the utilization of resolved side-band cooling [20,42], active feedback damping [27,28], and backaction evasion techniques [24,44]. A discussion of these techniques is outside the scope of this article.

V. MICROWAVE READOUT SYSTEM

A. Detection of frequency fluctuations

As described in the previous sections, a freely suspended sapphire bar is a unique physical object capable of supporting very-high-quality resonances, both mechanical and electromagnetic. It offers an opportunity to conduct a detailed study of the bar's mechanical resonances via their influence on the microwave resonances. In addition, one can investigate the inverse effects of the microwave readout on the SB's mechanical properties including the degeneration (cold damping) and regeneration (parametric excitation) of elastic vibrations [44,47].

This section describes a microwave readout system for monitoring the vibration state of a freely suspended sapphire bar. We expected that the sensitivity of the microwave readout would be sufficiently high to permit the very first observations of the bar's mechanical resonances excited by thermal fluctuations of the sapphire crystalline lattice.

There are at least two techniques, which can be employed for the microwave-assisted detection of elastic vibrations of the SB. Both techniques are widely used in the field of oscillator frequency stabilization for high-resolution measurements of fast frequency fluctuations [48,49]. In one case, the SB can be configured as a dispersive element of a microwave frequency discriminator. When driven from a fixed frequency signal source, the SB acts as a frequency-to-voltage converter, producing voltage varying synchronously with resonant frequency of a given WGM excited by the source. As a result, the task of analyzing a spectrum of a microwave signal is reduced to computing the fast Fourier transform of a sampled voltage at the discriminator output. Alternatively, the SB can serve as a bandpass filter of a self-exciting microwave loop oscillator [50]. This would "imprint" the spectrum of the SB mechanical normal modes on to the spectrum of the microwave signal. Once again, a frequency discriminator can be used to convert frequency fluctuations of the microwave signal into synchronous fluctuations of voltage. Performancewise, both of the above-mentioned techniques are identical; in each case the useful frequency fluctuations associated with elastic vibrations of the SB must compete with the same spurious fluctuations of the microwave readout electronics, and each technique, given some optimization, could potentially lead to spectral resolution close to the standard thermal noise limit [35].

B. Microwave sapphire-bar oscillator

Figure 10 shows a schematic diagram of a microwave loop oscillator based on the SB. The oscillator is frequency locked

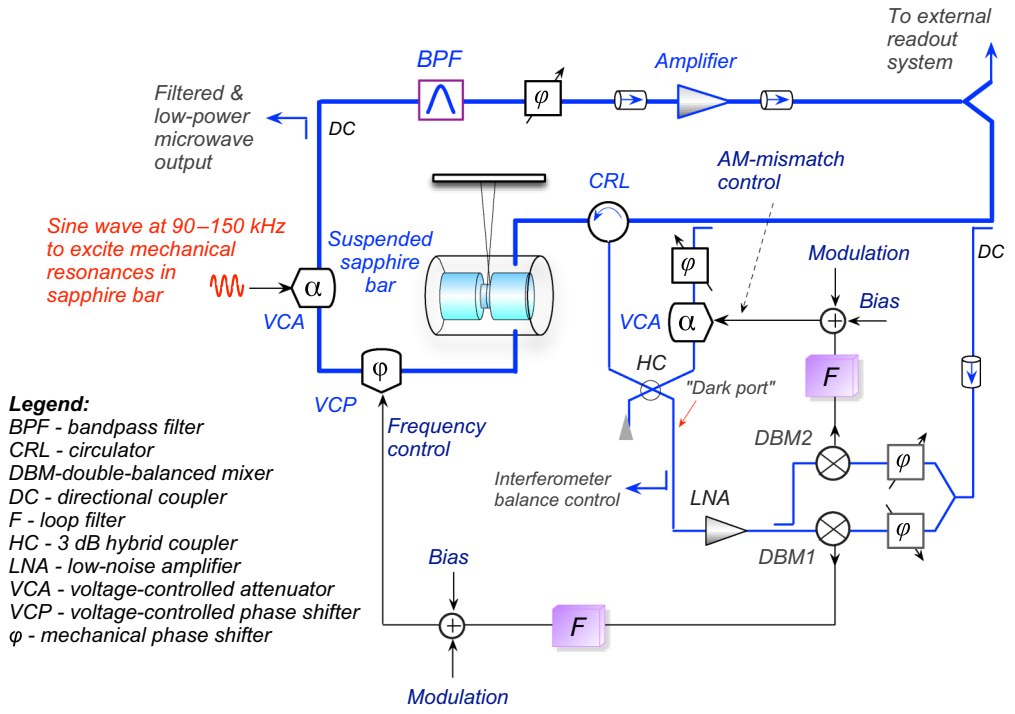

FIG. 10. (Color online) Schematic diagram of a frequency-stabilized microwave oscillator based on a suspended sapphire SB resonator excited in electromagnetic modes of a whispering gallery.

to a given WGM of the SB to facilitate detection of the useful frequency fluctuations. The spectrum of the free-running oscillator at Fourier frequencies of interest (∼100 kHz) is completely dominated by $1/f$ phase noise of the microwave loop amplifier. These spurious fluctuations are suppressed by the frequency lock (or frequency control) system, as explained below.

The key element of the oscillator frequency-control system is an ultrasensitive frequency discriminator. It consists of a microwave Mach-Zehnder interferometer with the suspended sapphire-bar resonator and a phase-sensitive readout system featuring low-noise amplifier (LNA) and a double-balanced mixer (DBM1 in Fig. 10). The microwave signal reflected from the SB interferes destructively with a fraction of the incident signal at the interferometer "dark port." This cancels the carrier of the difference signal while preserving noise modulation sidebands resulting from $1/f$ noise of the microwave loop amplifier. The residual noise at the dark port is amplified and demodulated to the baseband, producing an error voltage proportional to oscillator frequency fluctuations. The error voltage, after appropriate filtering, is applied to the electronic phase shifter (VCP) in the microwave loop. This steers the oscillator frequency to that of the resonator or, more precisely, to the frequency at which the carrier was suppressed, which is typically well within the resonator bandwidth. The frequency discriminator, loop filter, and VCP form the frequency-control loop. If the control loop gain is sufficiently high, the fidelity with which oscillator frequency follows that of the resonator is determined only by technical fluctuations in the electronics of the frequency discriminator. In this respect, interferometric frequency discriminators are far superior to their conventional counterparts, as they exhibit effective noise temperature close to the ambient temperature and are capable of handling much higher power levels [35].

It is not difficult to understand why frequency discriminators with the highest sensitivity are based on spindle-shaped sapphire crystals fixed rigidly inside the protective metal shields. The main reason for this is the low vibration sensitivity of such resonators, which makes the task of carrier suppression fairly straightforward. The situation is different in the case of the SB whose rocking motion upsets both amplitude and phase balance of the interferometer. To cope with the SB rocking motion, the oscillator in Fig. 10 features an additional feedback-control system charged with the task of minimizing amplitude mismatch between two signals interfering at the dark port. The error voltage for this feedback system is produced by the second mixer (DBM2) tuned in quadrature relative to the mixer of the frequency-control loop. The voltage-controlled attenuator (VCA) in the interferometer arm completes the feedback loop acting as an actuator of the amplitude mismatch control system.

The quadrature tuning of both DBMs is required to avoid the cross talk between the frequency- and amplitude-control loops. Yet the tolerances of such tuning proved to be not very stringent. For each control system, it was sufficient to roughly maximize the amplitude of the error signal (in response to some deliberately introduced perturbation) before closing the feedback loop.

An additional VCA in Fig. 10 is used to modulate the amplitude of the microwave signal. When the modulation frequency coincides with the frequency of mechanical resonance, parametric excitation of the normal mode ensues. This VCA was introduced when the refined suspension system made piezoelectric excitation of mechanical resonances ineffective.

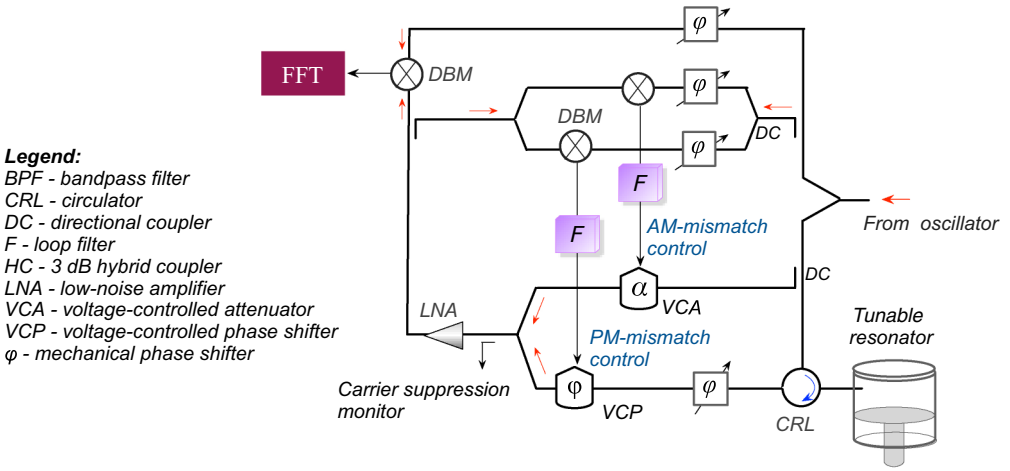

FIG. 11. (Color online) Schematic diagram of interferometric frequency discriminator with automatic carrier suppression.

C. Interferometric frequency discriminator

Approximately half of the power generated by the SB oscillator (Fig. 10) is diverted to the external frequency discriminator shown schematically in Fig. 11. It is practically identical to the previously described built-in discriminator of the SB oscillator; it also contains a microwave interferometer with actively controlled balance to cope with frequency variations of the input signal induced by the rocking motion of the SB and changes of ambient temperature.

The dispersive element of the external frequency discriminator is a cylindrical metal cavity with a Q factor of 15 000 and frequency tuning range of approximately 2 GHz. The wide tuning range of the cavity enables easy switching from one WGM of the sapphire bar to another, if one needs to investigate how a WGM of different polarization and azimuthal number responds to vibration.

Figure 12 shows spectra of phase fluctuations of various signal sources measured with the external frequency discriminator. The measurements were made at 9.774 GHz, corresponding to the excitation of the $\mathrm{WGH}_{15,1,1}$ mode of the SB.

The power spectral density of phase fluctuations S_ϕ was inferred from that of the voltage noise S_u via the relationship

$$S_\phi(F) = \frac{S_u(F)}{K_{\mathrm{FD}}^2}\left(\frac{1}{\Delta f_L^2} + \frac{1}{F^2}\right), \tag{18}$$

where F is the Fourier frequency, Δf_L is the half-loaded bandwidth of the cavity resonator, and K_{FD} is the frequency discriminator "dc sensitivity" measured at $F \ll \Delta f_L$.

The bottom trace in Fig. 12 shows the fit to the noise floor of the frequency discriminator expressed in the single sideband (SSB) units of dBc/Hz. The noise floor was measured with the cavity resonator replaced by a 50 Ω termination. Next we measured phase noise of a commercial frequency synthesizer (Agilent E8257C). The idea was to verify that the voltage-to-phase conversion procedure we followed was correct (our results proved to be consistent with the specs of the Agilent instrument). Finally, we characterized the phase noise of the SB oscillator, in both the free-running and the frequency-locked regimes. At Fourier frequencies $50\ \mathrm{kHz} < F < 500\ \mathrm{kHz}$, we observed more than 20 dB of phase noise suppression when the frequency lock was engaged.

As follows from Fig. 12, the SSB power spectral density of spurious phase fluctuations is -165 dBc/Hz at $F = 100$ kHz. The corresponding level of rms frequency fluctuations is

$$\delta f = F\sqrt{S_\phi(F)} \sim 8 \times 10^{-4}\ \mathrm{Hz}/\sqrt{\mathrm{Hz}}. \tag{19}$$

Recalling the frequency-displacement sensitivity of the sapphire bar ($f_z \sim 0.18\ \mathrm{MHz}/\mu\mathrm{m}$) yields the displacement noise floor: $\delta z \sim \delta f / f_z \sim 4 \times 10^{-15}\ \mathrm{m}/\sqrt{\mathrm{Hz}}$. This corresponds to the highest displacement sensitivity ever reported in experiments with sapphire-bar resonators as displacement transducers. Yet the level achieved is still approximately twice as large as the 127-kHz mode's elastic vibrations

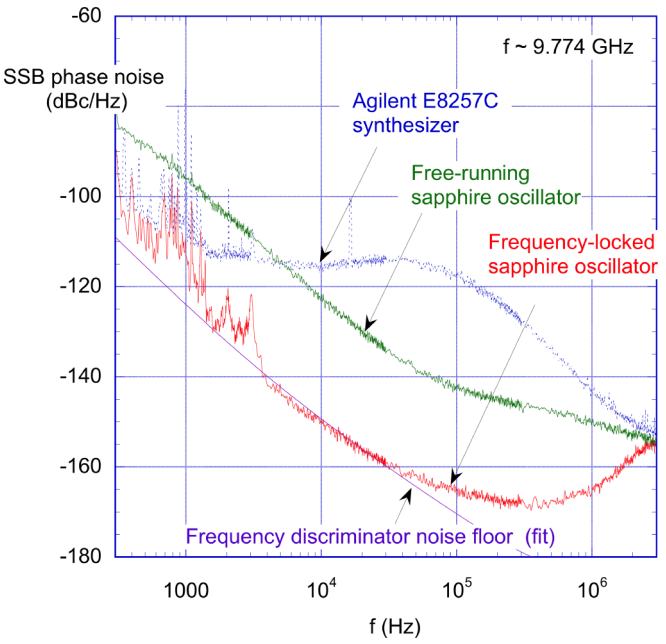

FIG. 12. (Color online) SSB phase noise spectra of various microwave signal sources measured with interferometric frequency discriminator with automatic carrier suppression. Power of the input signal is 19 dBm.

driven by thermal noise; hence, Brownian motion is currently unobservable with the present configuration.

At this stage, two questions can be posed: "What limits spectral resolution of the current experimental setup and how can it be improved?" In answering these questions, we, first of all, can single out two factors, which are almost equally responsible for the present level of displacement sensitivity. One of them is the relatively high level of phase noise of the frequency-locked microwave oscillator at $F \sim 100$ kHz. This is because the current frequency-control system starts losing gain at Fourier frequencies above 10 kHz. Solving this problem will involve the design of a new low-pass filter of the frequency feedback loop based on operational amplifiers with gain-bandwidth product exceeding 1 GHz.

The second limitation arises from the comparatively low electrical Q factor of the hollow metal cavity. We believe that at least an order of magnitude improvement in displacement sensitivity can be gained by replacing the hollow metal cavity with a sapphire loaded cavity resonator.

One "side effect" of resonator substitution is the loss of the wide frequency tunability. Yet some residual tunability would remain owing to the relatively high sensitivity of sapphire resonators to temperature ($df/dT \sim 0.5-0.7$ MHz/K, depending on the type of WGM used). Another complication of resonator substitution is related to the narrow bandwidths of sapphire resonators. An additional control system would be required to keep the sapphire resonator "in sync" with the incoming signal. We plan to address this issue by controlling microwave power dissipated in the sapphire crystal as in [36,51], where such a technique was used to enable the phase referencing of a "slave" sapphire oscillator to the "master." It should be remembered that the measurement sensitivity improves as a square root of the power of the SB oscillator.

A major advantage of the SB's dumbbell-shaped architecture is that it is, in fact, two electromagnetic oscillators, which are both undergoing the same mechanical fluctuations. One can easily imagine a cross-correlation scheme in which two readout systems as described above were constructed around either end of the SB. The primary mixer outputs of these readouts could then be cross correlated to eliminate uncorrelated electronic noise and boost the correlated mechanical signal, which would potentially allow never-before-seen levels of displacement sensitivity in such a system.

VI. PARAMETRIC EFFECTS

Parametric behavior will always arise when a driven resonant system is coupled to a second resonant system. A phase difference between the mechanical oscillator and the microwave resonance will produce either a damped or a driven system. As such, one can expect changes in the mechanical quality factor of a resonant optomechanical system as the "pump" signal is detuned from resonance. These effects have been well described in the past with various types of transducers [33,38,42,52,53]. The phenomenon, referred to as the "optical spring" effect, results from a Stokes/anti-Stokes process, whereby pumping above the optical resonance produces additional phonons; increasing the mechanical mode's effective temperature and Q factor, while pumping below resonance removes phonons from the system, effectively increasing losses and cooling the system [20]. There should also be a corresponding mechanical frequency shift associated with microwave pump detuning; however, it is predicted that it would be on the order of mHz, far below the resolution of the measurement technique used here, which relies upon a vector signal analyzer's "peak trace" function to record amplitude vs time.

Figure 13(a) demonstrates the optical spring effect for the 127-kHz mode of the SB resonator. These measurements were

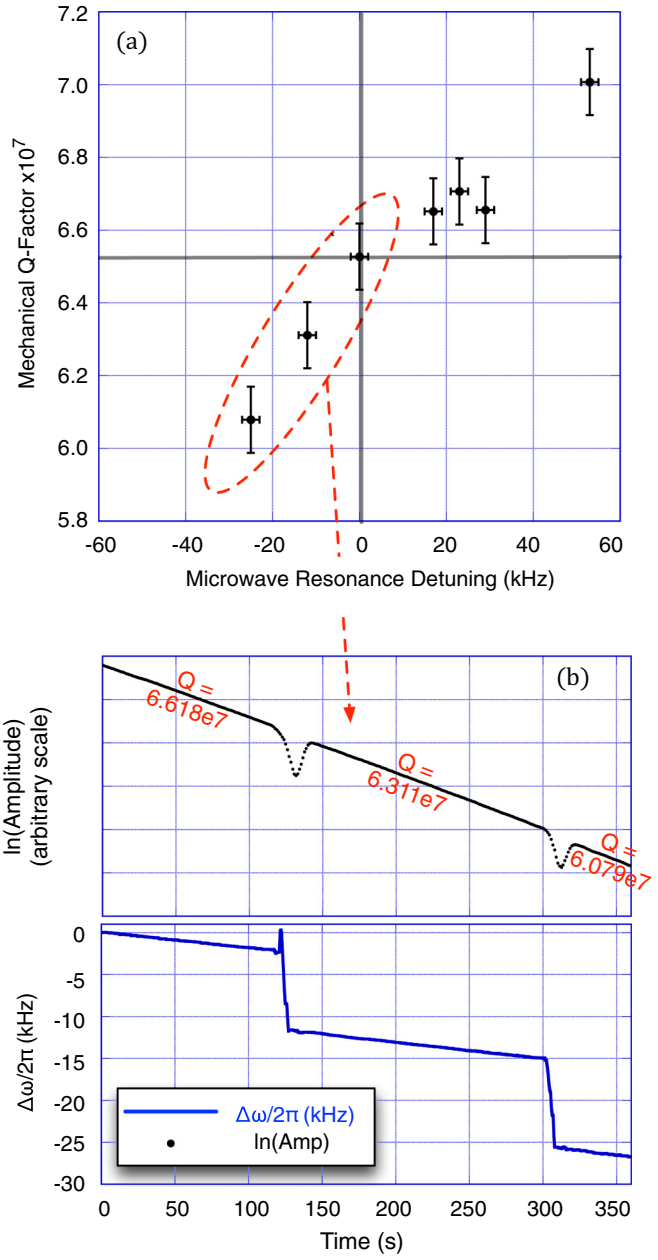

FIG. 13. (Color online) (a) Q factor vs input microwave frequency detuning. The circled data points are obtained from analyzing (b); a real-time ringdown measurement of the 127-kHz mechanical mode as negative detuning is increased during the measurement. The natural log of the amplitude is taken such that the time constant τ will be equal to the inverse of the gradient of a linear fit for each detuning value's data.

taken using a method depicted in Fig. 13(b), in which while the mechanical resonance rings down, the microwave detuning is changed from zero, and the resulting change in time constant is measured. Positive detuning results were also taken and the trials repeated. The transient response that can be seen immediately after a frequency shift in Fig. 13(b) is a result of the readout system requiring a rebalance.

Within the explored detuning range, $\Delta\omega_e < \Omega_m$; hence, one expects an approximately linear relationship between Q factor and detuning. The reason for this limited range is the restrictions placed by the bandwidth of the frequency-control system acting on the loop oscillator (see Sec. V). The loop oscillator and control system used to read out the mechanics of the SB complicate the microwave system beyond a simple LCR model.

The presence of parametric effects is a promising result for the system, as it is only through resolved sideband cooling [20] that a system such as the SB resonator could overcome thermal noise to reach quantum limited measurements and potentially the quantum ground state [20,42].

To date, we have achieved excellent agreement between modeled and measured frequencies of a variety of mechanical modes of the SB resonator and developed a robust method of mechanically exciting it via a piezoelectric shaker and via radiation pressure. The later method has also provided a method of calibrating the transducer's frequency sensitivity to displacement, df/dx, which has been measured to good agreement with predicted results. The mechanical Q factors have been optimized to a point at which they agree with maximum reported values at room temperature within limitations set by the quality of the sapphire, as does the $Q_m \times f$ product. In addition to this, if the SB resonator were cooled cryogenically, it would be equivalent to the best reported results for setting a limit on proposed quantum gravitational modifications to the standard Heisenberg uncertainty principle, potentially allowing a comparison of the consequences of various approaches to quantum gravity. Parametric backaction resulting in mechanical damping and excitation have also been observed. Finally, a microwave readout system has been constructed, which provides extremely low phase noise performance. This work provides an important enabling step for the next generation of kilogram-scale mechanical oscillator experiments designed to measure and test the standard quantum limit and potentially investigate the nature of quantum gravity by proving that novel architectures of sapphire systems can still produce state-of-the-art results.

ACKNOWLEDGMENTS

This work was supported by Australian Research Council Grants No. CE110001013 and No. FL0992016.

[1] K. L. Ekinci and M. L. Roukes, Nanoelectromechanical systems, Rev. Sci. Instrum. **76**, 061101 (2005).
[2] A. N. Cleland and M. L. Roukes, A nanometre-scale mechanical electrometer, Nature (London) **392**, 160 (1998).
[3] Y. T. Yang, C. Callegari, X. L. Feng, K. L. Ekinci, and M. L. Roukes, Zeptogram-scale nanomechanical mass sensing, Nano Lett. **6**, 583 (2006).
[4] A. K. Naik, M. S. Hanay, W. K. Hiebert, X. L. Feng, and M. L. Roukes, Towards single-molecule nanomechanical mass spectrometry, Nat. Nanotechnol. **4**, 445 (2009).
[5] H.-Y. Chiu, P. Hung, H. W. C. Postma, and M. Bockrath, Atomic-scale mass sensing using carbon nanotube resonators, Nano Lett. **8**, 4342 (2008).
[6] H. B. Peng, C. W. Chang, S. Aloni, T. D. Yuzvinsky, and A. Zettl, Ultrahigh frequency nanotube resonators, Phys. Rev. Lett. **97**, 087203 (2006).
[7] B. Lassagne, D. Garcia-Sanchez, A. Aguasca, and A. Bachtold, Ultrasensitive mass sensing with a nanotube electromechanical resonator, Nano Lett. **8**, 3735 (2008).
[8] P. Rabl, S. J. Kolkowitz, F. H. L. Koppens, J. G. E. Harris, P. Zoller, and M. D. Lukin, A quantum spin transducer based on nanoelectromechanical resonator arrays, Nat. Phys. **6**, 602 (2010).
[9] K. Stannigel, P. Rabl, A. S. Sørensen, P. Zoller, and M. D. Lukin, Optomechanical transducers for longdistance quantum communication, Phys. Rev. Lett. **105**, 220501 (2010).
[10] A. J. Leggett, Testing the limits of quantum mechanics: Motivation, state of play, prospects, J. Phys.: Condens. Matter **14**, R415 (2002).
[11] I. Pikovski, M. R. Vanner, M. Aspelmeyer, M. S. Kim, and C. Brukner, Probing Planck-scale physics with quantum optics, Nat. Phys. **8**, 393 (2012).
[12] F. Marin, F. Marino, M. Bonaldi, M. Cerdonio, L. Conti, P. Falferi, R. Mezzena, A. Ortolan, G. A. Prodi, L. Taffarello, G. Vedovato, A. Vinante, and J.-P. Zendri, Gravitational bar detectors set limits to Planck-scale physics on macroscopic variables, Nat. Phys. **9**, 71 (2013).
[13] A. F. Ali, S. Das, and E. C. Vagenas, Discreteness of space from the generalized uncertainty principle, Phys. Lett. B **678**, 497 (2009).
[14] A. F. Ali, S. Das, and E. C. Vagenas, Proposal for testing quantum gravity in the lab, Phys. Rev. D **84**, 044013 (2011).
[15] S. Das and E. C. Vagenas, Universality of quantum gravity corrections, Phys. Rev. Lett. **101**, 221301 (2008).
[16] G. M. Harry and the LIGO Scientific Collaboration, Advanced ligo: The next generation of gravitational wave detectors, Classical Quantum Gravity **27**, 084006 (2010).
[17] B. P. Abbott and the LIGO Scientific Collaboration, Ligo: The laser interferometer gravitational-wave observatory, Rep. Prog. Phys. **72**, 076901 (2009).
[18] T. Corbitt, D. Ottaway, E. Innerhofer, J. Pelc, and N. Mavalvala, Measurement of radiation-pressure-induced optomechanical dynamics in a suspended Fabry-Perot cavity, Phys. Rev. A **74**, 021802 (2006).
[19] J. Hofer, A. Schliesser, and T. J. Kippenberg, Cavity optomechanics with ultrahigh-Q crystalline microresonators, Phys. Rev. A **82**, 031804 (2010).

[20] J. D. Teufel, T. Donner, D. Li, J. W. Harlow, M. S. Allman, K. Cicak, A. J. Sirois, J. D. Whittaker, K. W. Lehnert, and R. W. Simmonds, Sideband cooling of micromechanical motion to the quantum ground state, Nature (London) **475**, 359 (2011).

[21] J. S. Bennett, L. S. Madsen, M. Baker, H. Rubinsztein-Dunlop, and W. P. Bowen, Coherent control and feedback cooling in a remotely coupled hybrid atom–optomechanical system, New J. Phys. **16**, 083036 (2014).

[22] K. H. Lee, T. G. McRae, G. I. Harris, J. Knittel, and W. P. Bowen, Cooling and control of a cavity optoelectromechanical system, Phys. Rev. Lett. **104**, 123604 (2010).

[23] C. R. Locke and M. E. Tobar, Measurement of the strain-induced coefficient of permittivity of sapphire using whispering gallery modes excited in a high-Q acoustic sapphire oscillator, Meas. Sci. Technol. **15**, 2145 (2004).

[24] C. Locke, Towards measurement of the standard quantum limit of a macroscopic harmonic oscillator, Ph.D. thesis, University of Western Australia, 2001.

[25] T. Corbitt, Y. Chen, F. Khalili, D. Ottaway, S. Vyatchanin, S. Whitcomb, and N. Mavalvala, Squeezed-state source using radiation-pressure-induced rigidity, Phys. Rev. A **73**, 023801 (2006).

[26] C. M. Caves, Quantum-mechanical noise in an interferometer, Phys. Rev. D **23**, 1693 (1981).

[27] T. Corbitt, C. Wipf, T. Bodiya, D. Ottaway, D. Sigg, N. Smith, S. Whitcomb, and N. Mavalvala, Optical dilution and feedback cooling of a gram-scale oscillator to 6.9 mK, Phys. Rev. Lett. **99**, 160801 (2007).

[28] T. Corbitt, Y. Chen, E. Innerhofer, H. Müller-Ebhardt, D. Ottaway, H. Rehbein, D. Sigg, S. Whitcomb, C. Wipf, and N. Mavalvala, An all-optical trap for a gram-scale mirror, Phys. Rev. Lett. **98**, 150802 (2007).

[29] B. C. Barish and C. Weiss, Ligo and the detection of gravitational waves, Phys. Today **52**, 44 (1999).

[30] T. Rocheleau, T. Ndukum, C. Macklin, J. B. Hertzberg, A. A. Clerk, and K. C. Schwab, Preparation and detection of a mechanical resonator near the ground state of motion, Nature (London) **463**, 72 (2010).

[31] J. D. Thompson, B. M. Zwickl, A. M. Jayich, F. Marquardt, S. M. Girvin, and J. G. E. Harris, Strong dispersive coupling of a high-finesse cavity to a micromechanical membrane, Nature (London) **452**, 72 (2008).

[32] J. C. Sankey, C. Yang, B. M. Zwickl, A. M. Jayich, and J. G. E. Harris, Strong and tunable nonlinear optomechanical coupling in a low-loss system, Nat. Phys. **6**, 707 (2010).

[33] D. G. Blair, D. E. McClelland, H. A. Bachor, and R. J. Sanderman, in *The Detection of Gravitational Waves*, edited by D. G. Blair (Cambridge University Press, Cambridge, UK, 1991).

[34] A. Schliesser and T. J. Kippenberg, Cavity optomechanics with whispering-gallery mode optical micro-resonators, in *Advances in Atomic, Molecular, and Optical Physics*, edited by E. A. Paul Berman and C. Lin (Academic Press, San Diego, CA, 2010), Vol. 58, Chap. 5, pp. 207–323.

[35] E. N. Ivanov and M. E. Tobar, Microwave phase detection at the level of 10^{-11} rad, Rev. Sci. Instrum. **80**, 044701 (2009).

[36] E. N. Ivanov and M. E. Tobar, Low phase-noise sapphire crystal microwave oscillators: Current status, IEEE Trans. Ultrason., Ferroelectr., Freq. Control **56**, 263 (2009).

[37] S. Rowan, G. Cagnoli, P. Sneddon, J. Hough, R. Route, E. K. Gustafson, M. M. Fejer, and V. Mitrofanov, Investigation of mechanical loss factors of some candidate materials for the test masses of gravitational wave detectors, Phys. Lett. A **265**, 5 (2000).

[38] C. R. Locke, M. E. Tobar, E. N. Ivanov, and D. G. Blair, Parametric interaction of the electric and acoustic fields in a sapphire monocrystal transducer with a microwave readout, J. Appl. Phys. **84**, 6523 (1998).

[39] T. Uchiyama, T. Tomaru, M. E. Tobar, D. Tatsumi, S. Miyoki, M. Ohashi, K. Kuroda, T. Suzuki, N. Sato, T. Haruyama, A. Yamamoto, and T. Shintomi, Mechanical quality factor of a cryogenic sapphire test mass for gravitational wave detectors, Phys. Lett. A **261**, 5 (1999).

[40] M. E. Tobar and A. G. Mann, Resonant frequencies of higher order modes in cylindrical anisotropic dielectric resonators, IEEE Trans. Microwave Theory Tech. **39**, 2077 (1991).

[41] J. Krupka, K. Derzakowski, A. Abramowicz, M. E. Tobar, and R. G. Geyer, Use of whispering-gallery modes for complex permittivity determinations of ultra-low-loss dielectric materials, IEEE Trans. Microwave Theory Tech. **47**, 752 (1999).

[42] M. Aspelmeyer, T. J. Kippenberg, and F. Marquardt, Cavity optomechanics, Rev. Mod. Phys. **86**, 1391 (2014).

[43] J. G. Hartnett, J. Jaeckel, R. G. Povey, and M. E. Tobar, Resonant regeneration in the sub-quantum regime — a demonstration of fractional quantum interference, Phys. Lett. B **698**, 346 (2011).

[44] V. B. Braginsky, V. P. Motrofanov, and V. I. Panov, *Systems with Small Dissipation* (Chicago University Press, Chicago, 1985).

[45] T. Uchiyama, D. Tatsumi, T. Tomaru, M. E. Tobar, K. Kuroda, T. Suzuki, N. Sato, A. Yamamoto, T. Haruyama, and T. Shintomi, Cryogenic cooling of a sapphire mirror-suspension for interferometric gravitational wave detectors, Phys. Lett. A **242**, 211 (1998).

[46] K. Numata, G. B. Bianc, N. Ohishi, A. Sekiya, S. Otsuka, K. Kawabe, M. Ando, and K. Tsubono, Measurement of the intrinsic mechanical loss of low-loss samples using a nodal support, Phys. Lett. A **276**, 37 (2000).

[47] P. Veitch, D. Blair, N. Linthorne, L. Mann, and D. Ramm, Development of a 1.5-tonne niobium gravitational radiational antenna, Rev. Sci. Instrum. **58**, 1910 (1987).

[48] M. E. Tobar, E. N. Ivanov, R. A. Woode, J. H. Searls, and A. G. Mann, Low noise 9-GHz sapphire resonator-oscillator with thermoelectric temperature stabilization at 300 Kelvin, Microwave Guided Wave Lett. IEEE **5**, 108 (1995).

[49] E. Ivanov, M. Tobar, and R. Woode, Microwave interferometry: Application to precision measurements and noise reduction techniques, IEEE Trans. Ultrason., Ferroelectr., Freq. Control **45**, 1526 (1997).

[50] D. B. Leeson, A simple model of feedback oscillator noise spectrum, Proc. IEEE **54**, 329 (1966).

[51] E. N. Ivanov, D. Mouneyrac, J.-M. Le Floch, M. E. Tobar, and D. Cros, Precise phase synchronization of a cryogenic microwave oscillator, Rev. Sci. Instrum. **81**, 064702 (2010).

[52] V. B. Braginsky, Physics experiments with test bodies, National Aeronautics and Space Administration, NASA technical translation F-672, 1972.

[53] M. E. Tobar, Gravitational wave detection and low noise sapphire oscillators, Ph.D. thesis, University of Western Australia, 1993.